Geotechnical Aspects of Underground Construction in Soft Ground – Yoo, Park, Kim & Ban (Eds)

Numerical investigation of the effect of cross walls in reducing ground settlement induced by deep excavation

C.Y. Ou
National Taiwan University of Science and Technology, Taipei, Taiwan

P.G. Hsieh
Hwa Hsia Institute of Technology, New Taipei City, Taiwan

S.C. Chien
Aletheia University, New Taipei City, Taiwan

ABSTRACT: This study presents the results from three-dimensional numerical analysis of two deep excavations with different installations of cross walls to demonstrate the effectiveness of cross walls in reducing lateral wall deflection and surface settlement. For simplifying analysis, an equivalent beam model suitable for two dimensional plane strain analysis is developed. Moreover, a simplified formula from the regression analysis of the three dimensional parametric study results is advanced. The above-mentioned two excavations were employed to demonstrate the proposed beam model and the simplified formula.

1 INTRODUCTION

The cross wall is a concrete wall built in an excavation transversely before excavation (Fig. 1). The function of the cross wall in mechanics is similar to the lateral strut, but it exists before excavation. It is expected to reduce the lateral wall deflection and ground settlement during excavation due to its high compressive strength and stiffness.

The behavior of diaphragm wall with cross walls is in nature three-dimensional. The objective of this paper is to present three-dimensional numerical analysis results of two excavation cases with cross walls to demonstrate the effectiveness of cross walls in reducing the wall deflection and surface settlement. A simplified plane strain analysis and simplified approach are also presented.

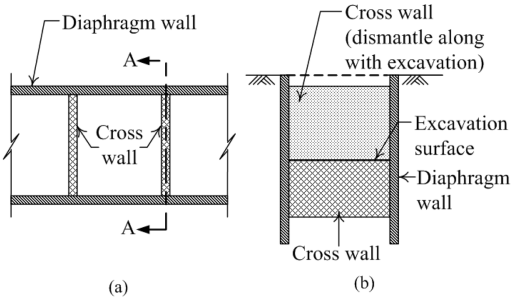

Figure 1. Schematic diagram of cross wall (a) plan (b) section.

2 THREE-DIMENSIONAL NUMERICAL ANALYSIS MODEL

FLAC^{3D} was used as a basic numerical analysis tool. Two analysis methods, the MCC/M-C analysis and the M-C/M-C analysis, were employed. With the MCC/M-C analysis, the modified Cam-clay (MCC) model and the Mohr-Coulomb (M-C) model were used to simulate the behavior of clay and sand, respectively. With the M-C/M-C analysis, the Mohr-Coulomb (M-C) model was adopted to simulate the behavior of clay as well as sand.

The parameters of the MCC model for clay were frictional constant (M), slope of normal consolidation line (λ), slope of elastic swelling line (κ), Poisson's ratio (ν). The parameters of the M-C model for clay were cohesion (c), friction angle (ϕ), Young's modulus (E), and Poisson's ratio (ν). Hsieh et al. (2013) details the derivation of the soil parameters and structural parameters used for excavations.

Two excavations with cross walls were used to demonstrate the three-dimensional numerical model. Figure 2 shows the layout and monitoring system of excavation case 1 (Ou et al. 2006). The excavation depth was 32.5 m, which was completed in 9 stages using the top-down construction method (Fig. 3). The thickness of the diaphragm wall (t_w) was 1.5 m and the average depth of the wall (H_t) was 57.5 m. Three cross walls of 1.0 m thick and 45 m deep with 26 m interval (L') were constructed. The cross walls between GL +0 m to GL −1.5 m were backfilled with the in-situ soil, between 1.5 m ~ 22 m were cast with the concrete

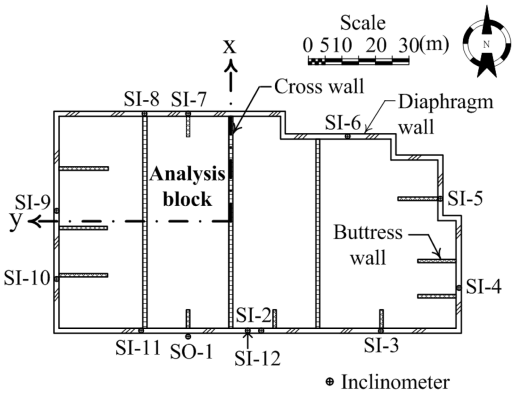

Figure 2. Excavation geometry and instrumentation for Case 1.

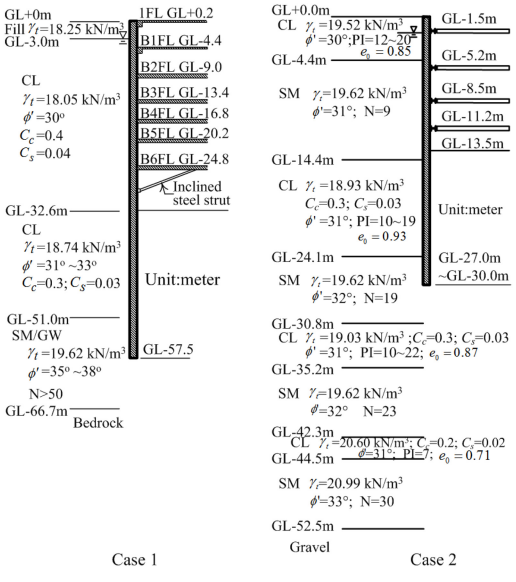

Figure 3. Excavation profiles for Cases 1 and 2.

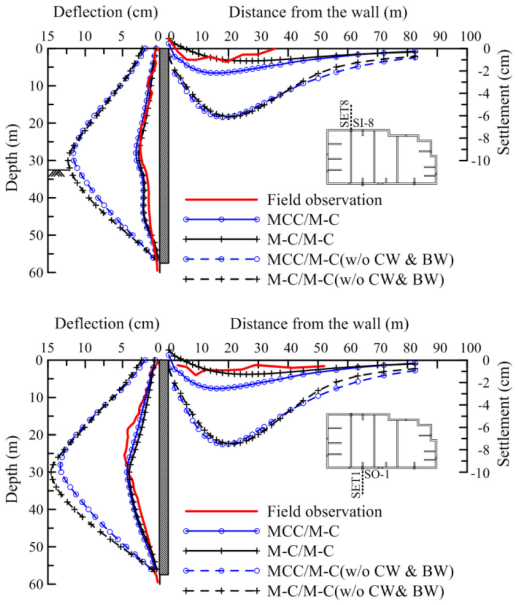

Figure 4. Comparison of observed and computed wall deflections and ground settlements at SI-8 and SO-1 for Case 1.

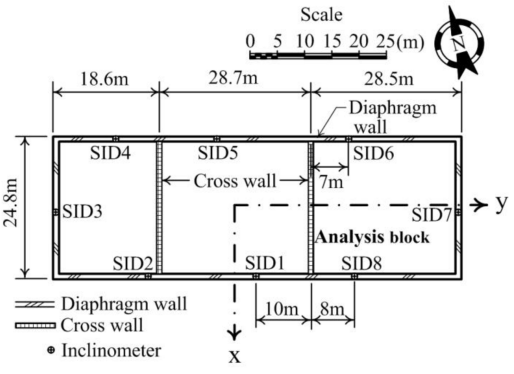

Figure 5. Excavation geometry and instrumentation for Case 2.

of 13.7 MPa and below 22 m were cast with the concrete of 24.0 MPa. Both the cross wall and cross wall were demolished with the excavation process.

Figure 4 shows the comparison of the observed wall deflections and surface settlements at SI-8 and SO-1 at final stages and those predicted from the MCC/M-C and M-C/M-C analysis. The analyses follow the exact construction sequence, allocation of cross walls and buttress walls. Analyses with the assumption of no cross walls and buttress walls (w/o CW & BW) were also performed and the results are shown in Figure 4. Both the MCC/M-C and M-C/M-C analyses resulted in a reasonable prediction for lateral wall deflection and surface settlement. The predicted wall deflections and surface settlements were much smaller than those without cross walls and buttress walls. Cross walls can substantially reduce lateral wall deflections and surface settlements. The maximum wall deflection and ground settlement at the final excavation stage were reduced by 67% to 77% and 78% to 81%, respectively.

Case 2 was a 13.5 m depth excavation. Figure 5 shows the excavation plan, which was 76 m long and 25 m wide. The excavation was completed in 5 stages using the bottom-up construction method (Fig. 3). The spacing between temporary steel strut was 4.6 m in the north-south direction and was 8.0 m in the east-west direction.

A 0.7 m thick and 27 m ~ 30 m deep diaphragm wall was adopted as the earth retaining structure. The compressive strength of the concrete (f_c') of the diaphragm wall was 27.5 MPa. Two cross walls of 0.7 m thick

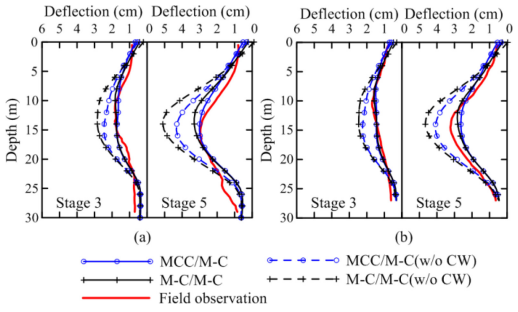

Figure 6. Comparison of wall deflections from observation and those from analysis for Case 2 (a) SID 1 (b) SID 8.

with 28.7 m in spacing were constructed in the north-south direction (Fig 5). The cross wall located at GL −13.5 m ~ GL −20.0 m, i.e. constructed starting from the excavation surface down to 6.5 m below it (Fig. 3). The f_c' of the cross wall was 27.5 MPa. It was backfilled with the in-situ soil above GL −13.5 m.

Figure 6 shows the comparison of the observed wall deflections at SID 1 and SID 8 at the 3th and the 5th excavation stages and those predicted from the MCC/M-C and M-C/M-C analysis. For comparison, analyses of Case 2 with the assumption of no cross walls (w/o CW) were performed and the results are also shown in the same figure. This figure shows that cross walls can reduce the lateral wall deflection significantly. The δ_{hm} at SID 1 and SID 8 were reduced by 33% and 37%, respectively.

Take the wall deflections at SO-1 in Case 1 and SID 1 in Case 2 for comparison because they were all located between two cross walls. If no cross walls were installed, the ratio of maximum wall deflection to excavation depth at SO-1 was around 41% to 44.9%, larger than that at SID 1, 32.1% to 37.8% because sand existed in Case 2. With cross walls, the ratio at SO-1 was reduced to be 13.6% to 12.6% while that at SID 1 from 22.3% to 24.5%. This is because Case 1 has smaller cross wall spacing and larger cross wall depth than Case 2.

3 SIMPLIFIED PLANE STRAIN NUMERICAL ANALYSIS MODEL

Considering that three-dimensional analysis is costly, a simplified plane strain analysis for excavations has been derived, as shown in Hsieh et al. (2012). Figure 7 shows that the lateral deflection of the diaphragm wall at a depth at the cross wall, i.e. section A-A, is denoted by $\delta_{h,0}$, at the midpoint of two cross walls, section B-B, denoted by $\delta_{h,mid}$, and at a distance, d, to the cross wall represented by $\delta_{h,d}$. The deflection of the diaphragm wall at a depth, subject to uniform pressure, can be decomposed into an elastic continuous beam supported by cross walls where the deflection

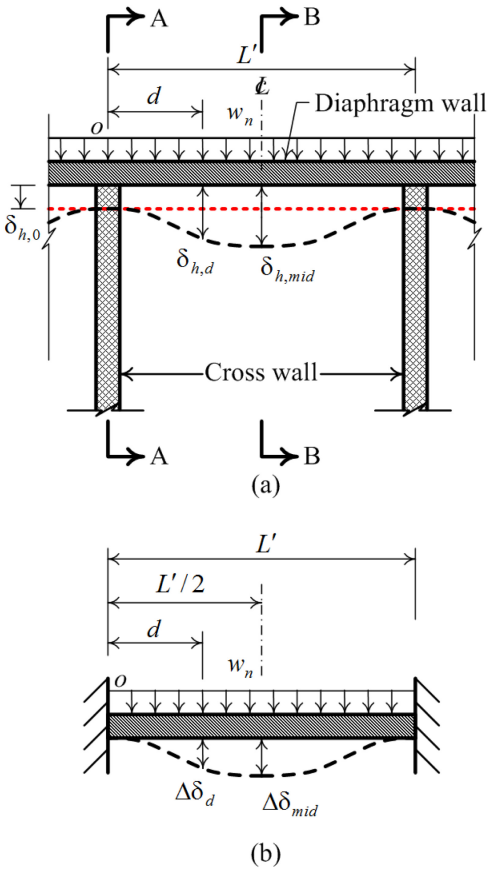

Figure 7. Decomposition of the diaphragm-cross wall system for a section into a continuous beam supported by cross walls and a fixed-end beam (a) A diaphragm wall with cross walls (b) A fixed-end beam.

of the beam is all equal to $\delta_{h,0}$ (Fig. 7(a)) and a fixed-end beam (Fig. 7(b)). The deflection of the fixed-end beam at any distance of d can be expressed by:

$$\Delta\delta_d = \frac{w_n L'^2 d^2}{24EI}\left(1 - \frac{2d}{L'} + \frac{d^2}{L'^2}\right) \quad (1)$$

where w_n is the earth pressure at a depth, L' is the cross wall interval, d is the distance to the cross wall, E is the Young's modulus of the beam and I is the moment of inertia.

Substituting $d = L'/2$ into Equation 1, we obtain:

$$\Delta\delta_{mid} = \frac{w_n L'^4}{384EI} \quad (2)$$

where $\Delta\delta_{mid}$ is the deflection of the fixed-end beam at the midpoint.

Therefore, the deflection of a diaphragm wall at a distance of d and at the midpoint between cross walls can be expressed, respectively, as (Fig. 7(a)):

$$\delta_{h,d} = \delta_{h,0} + \Delta\delta_d \quad (3)$$

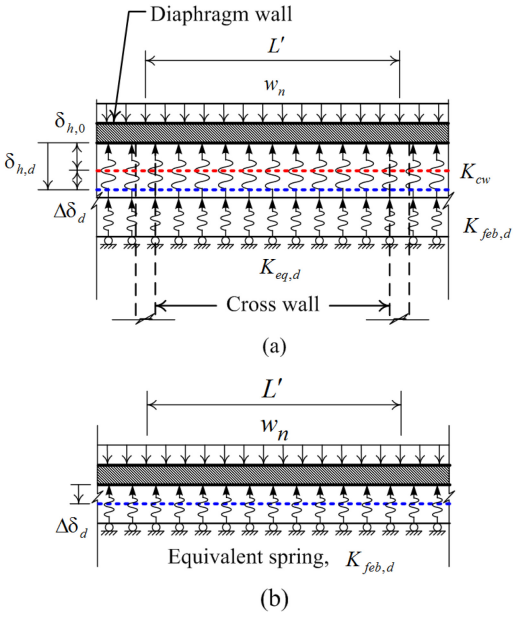

Figure 8. Simulation of the deflection behavior for the diaphragm-cross wall system for a section (a) A diaphragm wall with cross walls, (b) A fixed-end beam.

$$\delta_{h,mid} = \delta_{h,0} + \Delta\delta_{mid} \tag{4}$$

where $\delta_{h,d}$ is the deflection of the diaphragm wall at a distance of d from the cross wall and $\delta_{h,mid}$ is the deflection of the diaphragm wall at the midpoint between two cross walls.

Because the deflection of the continuous beam is all equal to $\delta_{h,0}$ (Fig. 7(a)), for plane strain analysis, the continuous beam supported by cross walls is simulated as it supported by springs (Fig. 8(a)). The spring stiffness per unit depth per unit length of the diaphragm wall, equivalent to the effect of cross walls across the intervals of L', is thus equal to:

$$K_{cw} = \frac{t_{cw}E_{cw}}{L'L_{cw}} \tag{5}$$

where K_{cw} is the equivalent spring stiffness per unit depth per unit length of the diaphragm wall; t_{cw} is the thickness of the cross wall; L_{cw} is the length of the cross wall.

For plane strain analysis of the fixed-end beam, as shown in Figure 7(b), the wall deflection at a distance of d can be simulated as a beam supported by springs whose deflection behavior is exactly the same as that section of the fixed-end beam. Assumed that the deflection of the fixed-end beam subject to a uniform pressure, w_n, at a distance of d is equal to $\Delta\delta_d$, the equivalent stiffness ($K_{feb,d}$) of springs supporting the continuous beam whose deflection behavior is exactly the same as that section would be:

$$K_{feb,d} = \frac{w_n}{\Delta\delta_d} \tag{6}$$

Table 1. The values of $K_{feb,d}$ and $K_{eq,d}$ for Case 1.

d (m)	$K_{feb,d}$ MN/m/m/m	$K_{eq,d}$ for $K_{cw} = 16.20$ MN/m/m/m	$K_{eq,d}$ for $K_{cw} = 21.44$ MN/m/m/m
0	∞	16.20	21.44
1	212.95	15.05	19.48
3	27.96	10.25	12.13
5	12.07	6.92	7.72
8	6.42	4.60	4.94
13	4.66	3.62	3.83

where $K_{feb,d}$ is the equivalent spring stiffness per unit depth per unit length of the diaphragm wall for a fixed end beam for the section at a distance of d (Fig. 8(b)).

Substituting $\Delta\delta_d$ in Equation 1 into Equation 6, we can obtain $K_{feb,d}$ as:

$$K_{feb,d} = \frac{24EI}{L'^2 d^2 - 2L' d^3 + d^4} \tag{7}$$

Substitute $d = L'/2$ into Equation 7, we can obtain the equivalent stiffness, $K_{feb,mid}$, at the midpoint as:

$$K_{feb,mid} = \frac{384EI}{L'^4} \tag{8}$$

By substituting the $\Delta\delta_d = w_n/K_{feb,d}$ and $\delta_{h,0} = w_n/K_{cw}$ into Equation 3, we can obtain the following expression as:

$$\frac{w_n}{K_{eq,d}} = \frac{w_n}{K_{cw}} + \frac{w_n}{K_{feb,d}} \tag{9}$$

where $K_{eq,d}$ is the equivalent stiffness of springs for the section of the diaphragm wall with cross walls at a distance of d per unit depth per unit length of the diaphragm wall.

Therefore, the deflection behavior of the diaphragm with cross walls at a distance of d (Fig. 7) can be considered as a beam supported by springs with the stiffness obtained from Equation 9, that is, the springs with the stiffness, K_{cw}, are connected in series with the springs with the stiffness, $K_{feb,d}$.

For case 1 validation, K_{cw} for the depth between GL −1.5 m to GL −22 m and GL −22 m to GL −45 m were computed to be 16.20 MN/m/m/m and 21.44 MN/m/m/m, respectively, in which $t_{cw} = 1.0$ m, $L' = 26$ m, $L_{cw} = B/2 = 33.05$ m and $E_{cw} = 13{,}917$ MPa (GL −1.5 m to GL −22 m) and 18,420 MPa (GL −22 m to GL −45 m). Table 1 lists $K_{eq,d}$ and its corresponding $K_{feb,d}$ for the sections at various distances where $d = 0$ denotes the section at cross wall, i.e. at SI-8 and $d = 13$ m the section at the midpoint of two cross walls, i.e. at SI-7 or SO-1.

The comparison of observed wall deflections at SI-8 and SO-1 for case 1 at the final stage and those predicted with the proposed equivalent beam model, along with the 3D analysis results is shown in Figure 9. The results from the analysis with the assumption of

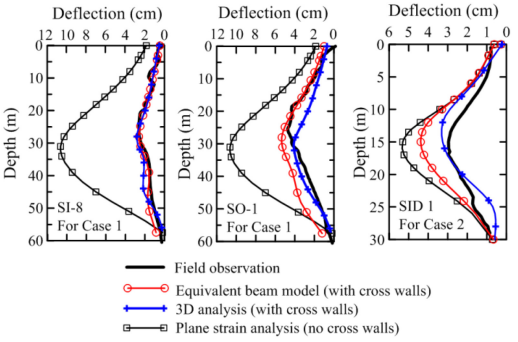

Figure 9. Comparison of observed and predicted wall deflections at SI-8 and SO-1 for Case 1 and SID1 for Case 2.

Table 2. The values of $K_{feb,d}$ and $K_{eq,d}$ for Case 2.

d (m)	$K_{feb,d}$ MN/m/m/m	$K_{eq,d}$ for $K_{cw}=38.78$ MN/m/m/m
0	∞	38.78
1	17.63	12.12
3	2.28	2.15
5	0.96	0.94
10	0.39	0.38
14.35	0.32	0.32

no cross walls are also shown in the same figure. The wall deflections predicted from the proposed equivalent beam model were very close to those from the field observation and 3D analysis results. This may be attributed to the fact that little difference in lateral wall deflection between the cross wall section and its nearby section exists.

For case 2 validation, the K_{cw} between GL −13.5 m to GL −20.0 m was found to be 38.78 MN/m/m/m in which $t_{cw}=0.7$ m, $L'=28.7$ m, $L_{cw}=B/2=12.4$ m and $E_{cw}=19{,}718$ MPa. Table 2 lists the equivalent stiffness for the sections at various distance and their corresponding $K_{feb,d}$. In the table, $d=10$ m denotes the section at SID 1 and $d=14.35$ m the central section.

The comparison of the observed wall deflections at SID 1 at the second to the final excavation stage and that predicted using the proposed equivalent beam model, along with the 3D analysis results is shown in Figure 9. The result from the analysis with the assumption of no cross wall is also shown in the same figure. The predicted wall deflection at SID 1 using the proposed equivalent beam model was very close to that of 3D analysis results and the assumption of no cross walls. Predicted wall deflections for with and without cross walls were also close to the field observations, implying that cross walls had little effect in restraining the lateral wall deflection. It is because cross walls in this case were set from the excavation surface down to −6.5 m below the excavation surface. There were no cross walls above the excavation surface, so the cross walls cannot provide a strong lateral resistance against the wall movement at the earlier stages of excavation.

4 SIMPLIFIED APPROACH

A series of three-dimensional parametric study for deep excavations without and with cross walls was performed, covering a wide range of excavation geometry and cross wall layouts. The variation of excavation parameters are: excavaiton depth (H) = 10 to 30 m, $s_u/\sigma'_v=0.25$ to 0.35, excavation width (B) = 20 to 80 m, the diaphragm wall thickness (t_w) = 0.6 to 1.4 m, the cross wall thickness (t_{cw}) = 0.6 to 1.0 m, and the cross wall interval (L') = 12 to 36 m. A simplified formula for predicting the maxium wall deflection for excavations without cross walls was first established as follows:

$$\delta_{hm,ps}/H=0.119e^{1.17X_e} \tag{10}$$

$$X_e=-0.0033H+0.011B-8.46s_u/\sigma'_v -0.000097S-0.000019S_a \tag{11}$$

where X_e is a synthetic parameter, inclusive of excavation geometry and soil properties, S is the wall system stiffness, S_a is axial stiffness of the lateral strut per unit length of the wall H and B are in meter, S_a is in MN/m and s_u/σ'_v, S are dimensionless.

Another simplified formula for predicting the maxium wall deflection for excavations with cross walls was then established as follows :

$$\delta_{hm,mid}=PSR_c\times\delta_{hm,ps}=0.11X_c^{3.59}\times\delta_{hm,ps} \tag{12}$$

$$X_c=0.36F_g^{-0.47}+2.23s_u/\sigma'_v+2.21S^{-0.28}+0.015R_a \tag{13}$$

$$F_g=\frac{BH}{L'^2} \tag{14}$$

$$R_a=\frac{S_a}{\frac{A_{cw}E_{cw}}{L'}} \tag{15}$$

where X_c is a synthetic parameter, inclusive of excavation geometry, cross wall properties and soil properties; F_g is the bay geometry factor, denoting the amount of soil excavated in a cross wall bay; R_a is the ratio of axial stiffness of cross walls to that of lateral struts per unit length of the diaphragm wall; A_{cw} is the cross sectional area of the cross wall over all levels of lateral strut, $A_{cw}=t_{cw}h_a$ where t_c and h_a are the cross wall thickness and average vertical spacing over all strut levels; E_{cw} is the Young's modulus of the cross wall.

To obtain the maximum wall deflection at the midpoint between two cross walls, the X_e should be first calculated using Equation 11 based on the parameters H, B, s_u/σ'_v, S and S_a. Then the maximum wall deflection for excavations without cross walls under the plane strain condition, $\delta_{hm,ps}$, was calculated by Equation 10. Then, the parameter X_c was calculated using Equation 13 with the additional parameters F_g and R_a estimated from Equations 14, 15, respectively. The $\delta_{hm,mid}$, can then be computed using Equation 12.

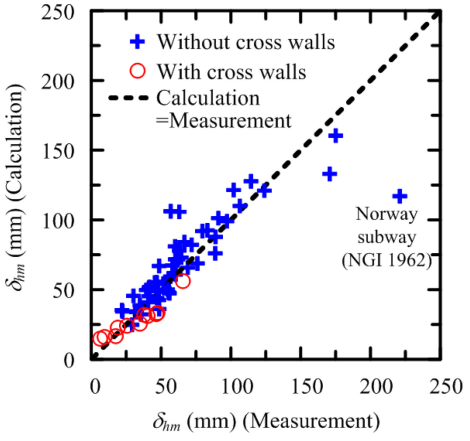

Figure 10. The measured and calculated maximum wall deflection for excavations without and with cross walls.

Since the inclinometer SO-1 in Case 1 was at the midpoint between two cross walls, the maximum wall deflection at SO-1 was used to illustrate the application of the simplified approach. According to Equations 10, 11, the parameters used to evaluate the $\delta_{hm,ps}$ are: $H = 32.5$ m, $B = 66.1$ m, $s_u/\sigma'_v = 0.34$, $S = 4156$, and S_a =11,041. The $\delta_{hm,ps}$ are computed to be 135 mm. According to Equations 12, 13, with two additional parameters, $F_g = 3.18$ and $R_a = 3.9$, the $\delta_{hm,mid}$ was calculated to be 34 mm, which was close to the measured wall deflection, 47 mm.

Moreover, 53 excavations without cross walls were used for more validation. The comparison between the maximum wall deflections from field observation and those from computed using Equations 10, 11 for excavations without cross walls are shown in Figure 10. The computed maximum wall deflections were very close to observed ones, except for a subway excavation in very soft clay, with unusual large wall deflections and its performance near the basal heave. The comparison between the maximum wall deflections from field observation and those from computed using Equations 12, 13 for 11 excavations with cross walls. The computed maximum wall deflections were very close to observed.

5 CONCLUSIONS

Compared with the assumption of no cross walls, cross walls can substantially reduce lateral wall deflections and surface settlements. For the case of cross walls constructed from the ground surface down to the wall bottom, the maximum wall deflection at the location of the cross wall and the midpoint between two cross walls were predicted to have a reduction of 77% and 67%, respectively. For the case of cross walls constructed from the excavation surface down to 6.5 m below it, the maximum wall deflection at the location of the cross wall and the midpoint between two cross walls were predicted to have a reduction of 67% and 29%, respectively. The percentage of reduction depends on the depth and interval of cross walls.

REFERENCES

Hsieh, P.G., Ou, C.Y. & Lin, Y.L. 2013. Three-dimensional numerical analysis of deep excavations with cross walls. Acta Geotechnica 8(1): 33–48.

Hsieh, P.G., Ou, C.Y. & Shih, C. 2012. A simplified plane strain analysis of the lateral wall deflection for excavations with cross walls. Canadian Geotechnical Journal 49: 1134–1146.

Ou, C.Y., Lin, Y.L. & Hsieh, P.G. 2006. Case record of an excavation with cross walls and buttress walls. Journal of GeoEngineering 1(2): 579–86.